Dose-dependent spatiotemporal responses of mammalian cells to an alkylating agent

Ann Rancourt[1, 2], Sachiko Sato[1], and Masahiko S. Satoh[2]*

[1]Glycobiology and Bioimaging Laboratory of Research Center for Infectious Diseases, and

[2]Laboratory of DNA Damage Responses and Bioimaging, CHUQ, Faculty of Medicine,

Laval University. 2705 Boulevard Laurier, Quebec, Quebec, G1V 4G2, Canada

*All correspondence should be addressed to Masahiko S. Satoh

TEL: 1-418-656-4141 ext. 47340

FAX: 1-418-654-2159

e-mail: Masahiko.sato@crchul.ulaval.ca

Abstract

Lethal doses of alkylating agents predominantly induce cell death, while cellular responses to lower doses may vary. However, understanding the responses in relation to the cytotoxic and carcinogenic effects of the agents have often been hindered by a lack of information on the spatiotemporal responses of exposed cells. We previously developed a single-cell lineage tracking system to characterize cultured cells at single-cell resolution. In the current study, we investigated the responses of cultured cervical cancer cells to three different doses of the alkylating agent *N*-methyl-*N*'-nitro-*N*-nitrosoguanidine (MNNG). A lethal dose of MNNG (5 μM) induced cell death immediately after exposure, while cells exposed to a sub-cytotoxic dose (2 μM) underwent cell death at various times following exposure, but remained capable of proliferation, implying that the cells could survive. Further analysis revealed that a non-cytotoxic dose (1 μM) of MNNG promoted the proliferation of previously identified putative cancer stem cells. MNNG can thus induce distinct dose-specific cellular responses, which may relate to the various cytotoxic, carcinogenic and anti-neoplastic effects of alkylating agents.

Introduction

Alkylating agents are potentially carcinogenic, but have also been used as anticancer drugs [1-6]. They produce alkylated DNA bases, which can in turn lead to various biological responses. For example, the alkylating agent *N*-methyl-*N′*-nitro-*N*-nitrosoguanidine (MNNG) produces methylated DNA bases, such as N^7-methyl guanine, which can be efficiently repaired by base excision repair [7-11]. However, poly(ADP-ribose) polymerase-1 is activated during the repair process and consumes intracellular NAD^+ [12-15]; exposure of cells to a high dose of MNNG may thus result in the depletion of NAD^+, leading to necrotic cell death (CD) [16], or in the synthesis of ADP-ribose polymers, which activate apoptotic CD [17]. Another MNNG-induced methylated DNA base, O^6-methyl guanine, which causes a G–to-A transitional mutation [2,18], may also lead to CD, even at low levels of MNNG [19]. Clinically relevant doses or low levels of alkylating agents, as used for anticancer treatment, also induce this type of CD [20]. O^6-methyl guanine-induced CD could be caused by the activation of mismatch correction to repair O^6-methyl G:T (or O^6-alkyl G:T) mismatches produced during the replication of DNA containing O^6-methyl G:C [21,22]. These observations suggest that cellular responses to alkylating agent exposure may vary according to the dose, and knowledge of the dose-specific responses of cancer cells to these agents is thus essential to understand their cytotoxic, carcinogenic and anti-neoplastic effects.

Cellular responses to alkylating agents occur spatiotemporally. It is therefore essential to investigate these responses using a suitable spatiotemporal method to enable the full elucidation of the biological effects of alkylating agents. Furthermore, the presence of cell-to-cell heterogeneity among cancer cells could cause non-uniform cellular responses to alkylating agents, and it is also necessary to investigate the effects using methods that can analyze individual cells. We have developed a novel chronological, single-cell lineage tracking analysis that can reveal significant cell-to-cell heterogeneity in cultured cancer cells [23]. We previously analyzed the cervical cancer-derived HeLa cell line using this method to record cellular events and movements of live cultured cells in a continuous manner, track individual cells, create a cell lineage database, and characterize the cell population using this database [23]. We

demonstrated that the fates of individual cells were diverse, indicating that the HeLa cell line comprises a highly heterogeneous population of cells. Moreover, some cells had a reproductive ability >20 times higher than other cells, suggesting that those cells (3.2%), tentatively referred to as putative cancer stem cells, may play a role in maintaining the HeLa cell population.

In this study, we investigated the different responses of cancer cells to alkylating agents by analyzing the responses of HeLa cells to exposure to non-cytotoxic, sub-cytotoxic and cytotoxic doses of MNNG using single-cell lineage tracking analysis.

Results

MNNG and live cell imaging

We exposed HeLa cells for 30 min to three different doses of MNNG as follows: non-cytotoxic (1 μM; dose at which cell proliferation was not reduced; MNNG1), sub-cytotoxic (2 μM; dose at which CD is induced but proliferation also occurs; MNNG2), and cytotoxic dose (5 μM: dose at which CD predominantly occurs; MNNG5). Non-treated cells (Control) and cells exposed to MNNG were cultured on a microscope stage and images were acquired every 10 min for 8500 min (141.7 h) to generate live cell imaging videos (see Supplementary Movies S1–4, and Movie S5 for exposure to lethal dose of MNNG, 40 μM). The recorded cells were identified and tracked over time to create a cell lineage database for use in subsequent analyses [23]. Cells identified at time point 1 were referred to as progenitor cells, and a data unit comprising cell-tracking data for a progenitor cell and its progeny was referred to as a cell lineage (Supplementary Figs. S1–4). Single-cell lineage tracking analysis was carried out using a multi-well chamber [23] to obtain simultaneous images of Control and exposed cells to allow accurate analysis of alterations in the exposed cells.

Effect of MNNG exposure on expansion of cell populations

We examined the effects of exposure to the different doses of MNNG on proliferation of HeLa cells (Fig. 1a). Growth curves were determined by calculating the number of progenitor cells or their progeny every 10 min. The numbers of Control and MNNG1 cells increased 6- and 7.3-fold, respectively, after 8500 min of cell culture (Fig. 1a). Curve-fitting analyses revealed that the cell proliferation measurements were performed with an accuracy of R = 98%. The numbers of progeny produced by each progenitor cell at 2000, 4000, 6000 and 8500 min were analyzed (Fig. 1b), and the differences between Control and MNNG1 cells at 4000, 6000 and 8500 min were significant ($p < 0.01$, $p < 0.0001$ and $p < 0.0001$, respectively) (Fig. 1a, b), suggesting that MNNG1 can promote cell

proliferation. Overall proliferation of MNNG2 cells had increased 1.5-fold at 8500 min (Fig. 1a), while division in some cells was increased up to 2500 min (Fig. 1c, indicated by the arrow). Given that clinically relevant doses of alkylating agents do not induce immediate cell cycle arrest [20-22], MNNG2 is likely to represent a clinically relevant dose equivalent. The number of cells decreased immediately after exposure to MNNG5, suggesting that this was a cytotoxic dose. These results suggest that the different doses of MNNG induce dose-specific responses in HeLa cells.

Effect of MNNG exposure on cell-doubling time

To gain further insights into the cellular responses induced by different doses of MNNG, we analyzed the effects of exposure on cell-doubling time. Cell-doubling times for each cell were calculated using the cell lineage database (Fig. 2). The mean cell-doubling time for Control cells was determined as 34.7 h by curve fitting using the Gaussian distribution (Fig. 2a). The cell-doubling time of cells exposed to MNNG1 was 3 h shorter than that of the Control cells (31.6 h) (Fig. 2b), indicating that MNNG1-exposed cells grew faster than Control cells and that MNNG1 promoted cell proliferation. The mean cell-doubling time was slightly decreased in cells exposed to MNNG2 (Fig. 2c), while the cell-doubling time was increased in cells exposed to MNNG5 (about 41.6 h; Fig. 2d). The increases or decreases in cell-doubling times of cells exposed to MNNG1, MNNG2 or MNNG5, respectively, were significant in relation to the Control cells (Fig. 2e). Overall, these confirmed that different doses of MNNG could induce specific responses in HeLa cells.

Effect of MNNG exposure on cellular events.

We previously reported that multipolar cell division (mainly tripolar cell division; TD [24,25]), CD and cell fusion (CF) occurred spontaneously during the growth of HeLa cells [23]. We therefore investigated the effects of the three doses of MNNG on these cellular events. The data were normalized by either the number of progenitor cells (number of cell lineages) (Fig 3a-c) or by the total number of cells (Fig.

3d-f). Cells exposed to MNNG1 showed a significant increase in TDs after normalization by the number of cell lineages (Fig. 3a), but not after normalization by the total number of cells (Fig. 3d). This suggests that MNNG1 may induce TD due to the MNNG1-promoted cell proliferation. TD, CD and CF were all reduced in cells exposed to MNNG5 after normalization by the number of cell lineages (Fig. 3a-c), but were all significantly increased when the number was normalized by the total number of cells (Fig. 3d-f). Cells exposed to MNNG2 showed a similar tendency (Fig. 3d-f), suggesting that MNNG2 and MNNG5 increase the frequency of TD, CD and CF. We then analyzed the relationships between CD and other cellular events (Fig. 3g). CD was induced in cells exposed to MNNG2 or MNNG5 following bipolar cell division (BD), TD and CF at similar frequencies. In contrast, significantly more CD events occurred following entry of MNNG5-exposed cells into mitosis (MI) compared with MNNG2-exposed cells, suggesting that abnormalities occurring prior to or during entry into MI were likely to be the major cause of CD induced by MNNG5. On the other hand, while CD occurred following MI in cells exposed to MNNG2, it was more frequently induced following BD (Fig. 3h). We therefore further analyzed CD induced in cells exposed to MNNG2.

Analysis of cells exposed to MNNG2

The numbers of BD and CD at each time point were plotted (Fig. 4a, b). The fact that the mean cell-doubling time of cells exposed to MNNG2 was 33.7 h (Fig. 2c) suggested that divisions of progenitor cells (first cell division) had likely occurred by 3000 min (50 h). We therefore determined the total numbers of BDs and CDs occurring before and after 3000 min. BD (n=148) occurred more frequently than CD (n=86) from 1–3000 min, thereby increasing the number of cells (Fig. 1c, black arrow). In contrast, CDs (n=255) were more frequent than BDs (n=306) from 3001 to 6000 min (Fig. 4a, b). Thus, unlike cells exposed to MNNG5 where CD was predominant to BD (Fig. 4c, d), cells exposed to MNNG2 retained the ability to proliferate, although the induction of CD inhibited the expansion of the cell population. It has been indicated that CD is induced in cells exposed to low levels of alkylating

agents after the first cell division [21,22]. We therefore investigated the time at which CD of the progeny occurred relative to the first (DV1), second (DV2) and third cell divisions (DV3) (Fig. 4e). CDs in Control cells occurred at DV1, DV2 and DV3 with similar frequencies (Fig. 4f), suggesting that CD occurred spontaneously in cells with a certain probability during the culture of HeLa cells. We then compared the number of CDs in Control and MNNG2-exposed cells (Fig. 4g), and found that MNNG2 induced CD in cells following DV1 and DV2, consistent with earlier observations [21,22]. We also investigated if CD occurred during S and G2 phases, as reported previously [21,22]. Because single-cell tracking was based on morphological observations, we were unable to measure the entry of cells into S or G2 phase directly. However, the analysis allowed us to determine the cell-doubling time of individual MNNG2-exposed cells precisely as 33 h (Fig. 2). We assumed that the duration of S1+G2+M phase is 13 h, and the duration of G1 phase was thus 20 h (Fig. 4h, right). We then calculated the numbers of CDs during the different phases. Although some CDs occurred during S+G2+M phases following DV1 (Fig. 4f) as reported [21,22], CDs occurring after the first division (DV1) occurred predominantly during G1. Overall, the responses of cells to sub-toxic doses of MNNG could vary, and MNNG2-induced CD could occur at various times and via various processes.

Analysis of cells exposed to MNNG1

MNNG1 promoted cell proliferation (Fig. 1a). We explored this effect further by analyzing the reproductive abilities of the progenitor cells and their progeny. The cell cycle was synchronized *in silico* to allow accurate determination of the number of progeny produced from a progenitor cell (Fig. 5a) [23]. In the *in silico* cell cycle-synchronization process, the first cell division was normalized at time point 1 (Fig. 5a), and the cell growth curves determined after the synchronization are shown in Fig. 5b. We then determined the number of progeny generated from one progenitor cell at 8500 min using the synchronized data (Fig. 5c). A single progenitor cell exposed to MNNG1 produced an average of 7.39 progeny cells, which was significantly higher than that produced by Control cells (6.08). We further

characterized the cells exposed to MNNG1 by grouping progenitor cells based on the number of progeny produced at 8500 min (Table 1). As shown in Table 1, 4.65% of Control cells produced ≥18 progeny cells (Group G), which represented a higher reproductive ability than other cells. In contrast, 11.68% of cells exposed to MNNG1 produced ≥18 progeny cells (Group G), suggesting that MNNG1 exposure increased the number of cells with high reproductive ability. Those cells had a significantly shorter cell-doubling time than Control cells (Table 1 and Fig. 5d). MNNG1 is therefore likely to stimulate the growth of a certain subpopulation of cells by increasing their reproductive ability and shortening the cell-doubling time.

Reproductive ability of granddaughter (GD) cells

We further investigated the cell population stimulated by exposure to MNNG1 by measuring the reproductive ability of GD cells. The cell cycle was synchronized *in silico* by normalizing to the cell-division time of progenitor cells at Time 1 (Fig. 5a) [23]. We first determined the number of progeny produced from a progenitor cell at 3500 min. Then, the GD cells of a progenitor cell were identified and the number of progeny produced from the GD cells after 3500 min from their first cell division of GD was determined. When a GD cell retained a similar reproductive ability to its progenitor cell, the GD cell was expected to produce similar numbers of progeny to its progenitor cell. The numbers of progeny produced from Control progenitor cells and cells exposed to MNNG1, and their GD cells, are shown in Fig. 6a. Both progenitor cells exposed to MNNG and their DG cells produced higher numbers of progeny than the respective Control cells, but there was no significant difference between the numbers of progeny produced from progenitor and DG cells, suggesting that DG cells retained a similar reproductive ability to its progenitor cells. We then reorganized the data shown in Fig. 6a according to the number of progeny produced from a progenitor cell (Fig. 6b), and the results suggested that MNNG1 increased the number of progenitor cells able to produce more than five progeny (Fig. 6b). We previously reported that HeLa cells contain a subpopulation with high reproductive ability,

involved in maintaining the HeLa cell population [23]. This population, referred to as putative cancer stem cells, accounts for 3%–7% [23]. The percentages of progenitor and GD cells that produced 7-8 progeny are shown in Fig. 6b. Control cells contained 3%–4% of these cells, while cells exposed to MNNG1 contained 9%–15%. A subpopulation of cells (6%–11%) with lower reproductive ability was thus converted into more highly reproductive cells by exposure to MNNG1. To identify the subpopulations converted into highly reproductive cells by exposure to MNNG1, we grouped progenitor cells according the number of progeny produced as follows: *A*, 1–2 progeny; *B*, 3–4 progeny; *C*, 5–6 progeny; and *D*, 7–8 progeny (Fig. 6b), and then determined the number of progeny produced from GD cells. The numbers of progeny produced from each group of progenitor cells (Fig. 6c, highlighted) indicated that some GD cells showed less reproductive ability than their progenitor cells, consistent with our previous report [23]. Most GD cells in Control group *B* produced four progeny, but this proportion was lower in cells exposed to MNNG1 (Fig. 6c), while the proportions of group *C* and *D* cells that produced more than five progeny were increased. These results suggest that MNNG1 produced more group *C* and *D* cells by stimulating the growth of cells that originally had the ability to produce four progeny (Group *B* cells).

Discussion

Cultured cells are composed of heterogeneous cell populations [23] and their responses to exogenously added substances occur spatiotemporally; it is therefore essential to analyze cells using a chronological method that can reveal the responses of individual cells to such substances, to allow the accurate evaluation of their effects on the cells. In the present study, we investigated the responses induced in cells by exposure to different doses of MNNG using chronological analysis, i.e. single-cell lineage tracking analysis. To the best of our knowledge, this represents the first use of this analysis to characterize the responses of cells to an alkylating agent, MNNG, and to demonstrate that MNNG over a five-fold dose range induced significantly different cellular responses. Given that alkylating agents are used as anticancer drugs [1-6], a better understanding of the responses of cells to MNNG could help to improve cancer therapy using these agents.

A cytotoxic dose of MNNG (MNNG5) inhibited cell growth by inducing CD. The fact that most CDs occurred following the entry of cells into MI suggested that MNNG5 may induce CD by perturbation of DNA replication caused by the formation of large amounts of DNA damage.

MNNG2 also inhibited cell growth, though cell populations exposed to MNNG2 could expand about 1.5-fold after 8500 min of culture. Although MNNG2 induced CD, cells exposed to MNNG2 retained the ability to proliferate, leading to the 1.5-fold expansion of the cell population, and some cells even showed resistance to the exposure. Regarding the induction of CD by MNNG2, low levels of alkylating agents have been reported to induce CD after BD of exposed cells, due to the repair of O^6-alkyl G:T mismatches produced by replication of O^6-alkyl G:C, by mismatch correction [19,21,22,26-30]. Indeed, we observed the induction of CD following BD in exposed progenitor cells, though CD also occurred following the entry of cells into MI, after BD of daughter or GD cells, and during G1 and S+G2+MI phases. Given that the responses of cells to this level of alkylating agents could vary depending on the reproductive ability of the cells and other phenotypical characteristics, e.g. their ability to repair DNA damage, their ability to survive or induce CD, may be affected by various factors. Some reports have

suggested that CD occurs during S or G2 phases of daughter cells produced by BD of exposed progenitors, or following DV3 [19,21,22,26-30]; however, it is likely that these studies only revealed responses of specific sub-populations of cells to exposure. Spatiotemporal information on cellular responses to alkylating agents may thus help to eliminate ambiguities associated with cellular heterogeneities, and allow more accurate characterization of the effects of alkylating agents on cancer cells.

MNNG1 promoted cell proliferation, associated with an increased occurrence of TD. This increase was caused by an increase in the population of well-growing cells referred to as putative cancer stem cells [23]. However, if Control HeLa cells contain a constant number of these putative cancer stem cells, the increased portion found in cells exposed to MNNG1 must be derived from other sub-populations. Our results suggested that MNNG1 converted less-reproductive cells or dormant putative cancer stem cells into cells with a higher reproductive ability. Although it is not yet clear if the cancer stem cell-like cells found in HeLa cell cultures are similar to cancer stem cells identified in cancer tissues, MNNG1 could promote the growth of those cells. Interestingly, MNNG is known to induce hyperplasia in rodents [31,32], suggesting that the observed promotion of cell growth by MNNG1 *in vitro* may also occur *in vivo* by stimulating the growth of tissue-specific or dormant stem cells. Regarding TD, the MNNG1-induced increase in TD could lead to alterations in cell ploidy, as the division of one cell into three cells leads to the random distribution of chromosomes to the progeny cells [25,33]. The progeny produced as a result of TD are typically fragile [24] and HeLa cells produced by TD rarely survive (see Supplementary Figs.). However, if a progeny cell inherits a set of chromosomes that are sufficient for viability, this could result in the formation of an aneuploidic cell population. The German scientist Theodor Boveri proposed about 100 years ago that this type of division could cause human cancers, and aneuploidy was considered to be the main cause of malignant transformation prior to the proposal of the gene mutation hypothesis [34,35]. Although the carcinogenic roles of promotion of cell proliferation, activation of dormant cells and the promotion of TD by exposure to non-cytotoxic doses of MNNG remain unclear,

substances that act as growth promoters at low doses have been proposed as likely human carcinogens [36]. Analyzing the responses of cultured mammalian cells to a low dose of carcinogenic substances using single-cell lineage tracking may thus provide clues to further our understanding of the process of human carcinogenesis.

Materials and Methods

HeLa cells were purchased from ATCC and cultured in DMEM containing 10% fetal bovine serum in a humidified 5% CO^2. To plate cells onto a coverglass Lab-Tek 8 well chamber, 50 µl of HeLa suspension containing 3500 cells were placed at the center of each well and left until cells attached to the coverglass surface. Then, 0.75 ml of culture medium was added to each well. Cells were used for live cell imaging 18 h after the plating. HeLa cells were treated with various concentration of MNNG (Sigma-Aldrich) for 30 min in serum free DMEM.

Long-term live cell imaging and data analysis

Quorum WaveFX Spinning Disc Confocal System (Quorum Technologies Inc., Canada) with Leica microscope controlled by Volocity v4.0 was used for long-term live cell imaging. Differential interference contrast (DIC) images were taken through HCX PL APO 40x oil objectives (NA=1.25) by using a Halogen lamp as a light source. Cells that were grown on a coverglass Lab-Tek 8 well chamber were then placed on a microscope stage and were cultured using an environmental chamber at 37ºC with 7.5% humidified CO_2 (Pathology Devices Inc, MD). In each well, a two-dimensional image acquisition array (filed of views: FOVs) was made to cover the area of interest [23]. XY positions of FOVs were then registered using Volocity v4.0. DIC images were captured every 10 min from + 10 to – 10 µm of the focal plan at every 1 µm using piezo focus drive. Exposure time was 34 msec. To make time-lapse movies, focused images were selected from 21 *z*-plane image files using Volocity v4.0. After the selection, files containing focused image were assembled into a movie using QuickTime player Pro. Panorama views of time point = 1 were prepared and cell lineage numbers were assigned to cells in a selected area [23]. After assigning the cell lineage numbers, each cell was tracked using QuickTime player Pro and the time points that MI, BD, CD, CF, and CD occurred in each cell were determined. To draw cell lineage maps and process data, C/C++ programs were written. At least two independent experiments were performed to confirm reproducibility. Then, 200-300 progenitor cells

and their progeny were tracked.

Statistical analyses

Student's *t*-tests (unpaired and two-tailed) were performed using Prism 7. Statistical data is summarized in the Supplementary Data Set.

Acknowledgements

We like to acknowledge Ms. Julie-Christine Lévesque, and the Bioimaging Platform of Research Center for Infectious Diseases, CRCHU de Québec for the technical support of microscopes. This work was supported by the Canadian Foundation for Innovation for MSS and SS.

Author contributions

M.S.S. and S.S. designed this work, performed the experiments and wrote the paper. A.R. performed experiments and single-cell tracking analysis.

References

1 IARC monographs on the evaluation of the carcinogenic risk of chemicals to humans: some N-nitroso compounds. *IARC Monogr Eval Carcinog Risk Chem Man* **17**, 1-349 (1978).

2 Eadie, J. S., Conrad, M., Toorchen, D. & Topal, M. D. Mechanism of mutagenesis by O6-methylguanine. *Nature* **308**, 201-203 (1984).

3 Harris, C. C. The carcinogenicity of anticancer drugs: a hazard in man. *Cancer* **37**, 1014-1023 (1976).

4 Schabel, F. M., Jr. Nitrosoureas: a review of experimental antitumor activity. *Cancer Treat Rep* **60**, 665-698 (1976).

5 Sukumar, S., Notario, V., Martin-Zanca, D. & Barbacid, M. Induction of mammary carcinomas in rats by nitroso-methylurea involves malignant activation of H-ras-1 locus by single point mutations. *Nature* **306**, 658-661 (1983).

6 Sukumar, S. *et al*. A transforming ras gene in tumorigenic guinea pig cell lines initiated by diverse chemical carcinogens. *Science* **223**, 1197-1199 (1984).

7 Drablos, F. *et al*. Alkylation damage in DNA and RNA--repair mechanisms and medical significance. *DNA Repair (Amst)* **3**, 1389-1407 (2004).

8 Kubota, Y. *et al*. Reconstitution of DNA base excision-repair with purified human proteins: interaction between DNA polymerase beta and the XRCC1 protein. *EMBO J* **15**, 6662-6670 (1996).

9 Sedgwick, B., Bates, P. A., Paik, J., Jacobs, S. C. & Lindahl, T. Repair of alkylated DNA: recent advances. *DNA Repair (Amst)* **6**, 429-442 (2007).

10 Singer, B., Fraenkel-Conrat, H., Greenberg, J. & Michelson, A. M. Reaction of nitrosoguanidine (N-methyl-N'-nitro-N-nitrosoguanidine) with tobacco mosaic virus and its RNA. *Science* **160**, 1235-1237 (1968).

11 Strauss, B., Scudiero, D. & Henderson, E. The nature of the alkylation lesion in mammalian cells. *Basic Life Sci* **5A**, 13-24 (1975).

12 Lindahl, T., Satoh, M. S., Poirier, G. G. & Klungland, A. Post-translational modification of poly(ADP-ribose) polymerase induced by DNA strand breaks. *Trends Biochem Sci* **20**, 405-411 (1995).

13 Luo, X. & Kraus, W. L. On PAR with PARP: cellular stress signaling through poly(ADP-ribose) and PARP-1. *Genes Dev* **26**, 417-432 (2012).

14 Satoh, M. S. & Lindahl, T. Role of poly(ADP-ribose) formation in DNA repair. *Nature* **356**, 356-358 (1992).

15 Ray Chaudhuri, A. & Nussenzweig, A. The multifaceted roles of PARP1 in DNA repair and chromatin remodelling. *Nat Rev Mol Cell Biol* **18**, 610-621 (2017).

16 Burkle, A. Physiology and pathophysiology of poly(ADP-ribosyl)ation. *Bioessays* **23**, 795-806 (2001).

17 Yu, S. W. *et al*. Mediation of poly(ADP-ribose) polymerase-1-dependent cell death by apoptosis-inducing factor. *Science* **297**, 259-263 (2002).

18 Myrnes, B., Giercksky, K. E. & Krokan, H. Repair of O6-methyl-guanine residues in DNA takes place by a similar mechanism in extracts from HeLa cells, human liver, and rat liver. *J Cell Biochem* **20**, 381-392 (1982).

19 Schroering, A. G. *et al*. Prolonged cell cycle response of HeLa cells to low-level alkylation exposure. *Cancer Res* **69**, 6307-6314 (2009).

20 Friedman, H. S., Kerby, T. & Calvert, H. Temozolomide and treatment of malignant glioma. *Clin Cancer Res* **6**, 2585-2597 (2000).

21 Stojic, L. *et al*. Mismatch repair-dependent G2 checkpoint induced by low doses of SN1 type methylating agents requires the ATR kinase. *Genes Dev* **18**, 1331-1344 (2004).

22 Yoshioka, K., Yoshioka, Y. & Hsieh, P. ATR kinase activation mediated by MutSalpha and MutLalpha in response to cytotoxic O6-methylguanine adducts. *Mol Cell* **22**, 501-510 (2006).

23 Sato, S., Rancourt, A., Sato, Y. & Satoh, M. S. Single-cell lineage tracking analysis reveals that an established cell line comprises putative cancer stem cells and their heterogeneous progeny. *Sci Rep* **6**, 23328 (2016).

24 Ganem, N. J., Godinho, S. A. & Pellman, D. A mechanism linking extra centrosomes to chromosomal instability. *Nature* **460**, 278-282 (2009).

25 Shi, Q. & King, R. W. Chromosome nondisjunction yields tetraploid rather than aneuploid cells in human cell lines. *Nature* **437**, 1038-1042 (2005).

26 Hawn, M. T. *et al*. Evidence for a connection between the mismatch repair system and the G2 cell cycle checkpoint. *Cancer Res* **55**, 3721-3725 (1995).

27 Iyer, R. R., Pluciennik, A., Burdett, V. & Modrich, P. L. DNA mismatch repair: functions and mechanisms. *Chem Rev* **106**, 302-323 (2006).

28 Schroering, A. G., Edelbrock, M. A., Richards, T. J. & Williams, K. J. The cell cycle and DNA mismatch repair. *Exp Cell Res* **313**, 292-304 (2007).

29 Tominaga, Y., Tsuzuki, T., Shiraishi, A., Kawate, H. & Sekiguchi, M. Alkylation-induced apoptosis of embryonic stem cells in which the gene for DNA-repair, methyltransferase, had been disrupted by gene targeting. *Carcinogenesis* **18**, 889-896 (1997).

30 Wang, Y. & Qin, J. MSH2 and ATR form a signaling module and regulate two branches of the damage response to DNA methylation. *Proc Natl Acad Sci U S A* **100**, 15387-15392 (2003).

31 Chopra, D. P. & Wilkoff, L. J. Inhibition and reversal by beta-retinoic acid of hyperplasia induced in cultured mouse prostate tissue by 3-methylcholanthrene or N-methyl-N'-nitro-N-nitrosoguanidine. *J Natl Cancer Inst* **56**, 583-589 (1976).

32 Chopra, D. P. & Wilkoff, L. J. Reversal by vitamin A analogues (retinoids) of hyperplasia induced by N-methyl-N'-nitro-N-nitrosoguanidine in mouse prostate organ cultures. *J Natl Cancer Inst* **58**, 923-930 (1977).

33 Gisselsson, D. *et al*. When the genome plays dice: circumvention of the spindle assembly checkpoint and near-random chromosome segregation in multipolar cancer cell mitoses. *PLoS One* **3**, e1871 (2008).

34 Boveri, T. Concerning the origin of malignant tumours by Theodor Boveri. Translated and annotated by Henry Harris. *J Cell Sci* **121 Suppl 1**, 1-84 (2008).

35 Holland, A. J. & Cleveland, D. W. Boveri revisited: chromosomal instability, aneuploidy and tumorigenesis. *Nat Rev Mol Cell Biol* **10**, 478-487 (2009).

36 Cohen, S. M. & Ellwein, L. B. Cell proliferation in carcinogenesis. *Science* **249**, 1007-1011 (1990).

Figure legends

Fig. 1 Effect of MNNG exposure on cell proliferation.

a. The number of cells at each time point was determined using the cell lineage database. The initial number of cells was normalized by 100. Curves were fitted using non-linear regression-curve fitting (Prism 7). **b.** The numbers of cells produced from each progenitor cell at the 2000, 4000, 6000 and 8500 min time points were calculated and analyzed by Student's *t*-tests; *p<0.05, **p<0.01, ***p<0.001 and ****p<0.0001 in relation to Control. Mean ± standard error (SEM) are shown. The p values are also shown in **a**. **c.** Growth curves for the time points from 1 to 4000 min are shown. Arrow indicates the time point at which the number of cells exposed to MNNG2 reached the maximum.

Fig. 2 Analysis of cell-doubling time.

Cell-doubling times distribution of Control cells (**a**) and cells exposed to MNNG1 (**b**), MNNG2 (**c**) and MNNG5 (**d**) are shown. The mean cell-doubling times and standard deviations were calculated (**a**, **b** and **c**) using the Gaussian distribution (Prism 7). **e.** The cell-doubling times of each group of cells were determined and analyzed by Student's *t*-tests; **p<0.01, ***p<0.001 and ****p<0.0001 in relation to Control. Mean ± SEMs are shown. Cell-doubling time shown in **d** was calculated using the cell-doubling times of MNNG5, because a Gaussian distribution could not be performed.

Fig. 3 Numbers of TD, CD and CF in cells exposed to MNNG.

Data in **a-c** were normalized by the number of progenitor cells (number of cell lineages) and data in **d-f** by the total number of cells. The numbers of TD (**a, d**), CD (**b, e**) and CF (**c, f**) were determined using the cell lineage database. **g-h.** The numbers of CD that occurred following BD, TD, CF or MI are shown. **a-h.** Student's *t*-tests were performed in relation to Control (**a-g**) or BD > CD (**h**); ns: not significant, and *p<0.05, **p<0.01, ***p<0.001 and ****p<0.0001. Mean ± SEMs are shown.

Fig. 4 Analysis of cells exposed to MNNG2 or MNNG5.

The numbers of BD (**a, c**) and CD (**b, d**) occurring at each time point in cells exposed to MNNG2 (**a, b**) or MNNG5 (**c, d**) are plotted. The total numbers of BD and CD that occurred before and after 3000 min were determined. **e.** CDs occurring following the division of progenitor cells (DV1), daughter cells (DV2) and GD cells (DV3) were determined. **f-g.** The number of CDs that occurred following DV1, DV2 and DV3 were normalized by the number of DV1, DV2 and DV3, respectively. **f.** Mean ± SEMs are shown. There was no statistical significance in relation to DV1 > CD. **g.** Student's *t*-tests were performed; *p<0.05, ***p<0.001 and ****p<0.0001 in relation to Control. Mean ± SEMs are shown. **h.** We assumed that the cell-doubling time of the cells exposed to MNNG2 was 33 h, the duration of S1, G2 and M phases was 13 h, and the duration of G1 was thus 20 h. CD occurring during G1 and S+G2+M phases was determined. Mean ± SEMs are shown. Student's *t*-tests were performed; ***p<0.001 in relation to G1.

Fig. 5 Analysis of progeny produced from Control progenitor and MNNG1-exposed cells.

a. The cell cycle was synchronized *in silico*. The time point when the progenitor cells divided was normalized as Time 1 (blue arrowhead). Blue line indicates the time point 3500 min after the division. GD cells are indicated by green arrowhead. The red line shows the time point 3500 min after the division of GD cells (red arrowhead). **b.** Cell growth curves determined after synchronization. **c**. The number of progeny produced from a progenitor at 8500 min was determined using an *in silico* synchronized cell lineage database and Student's *t*-tests were performed; *p<0.05 and ****p<0.0001 in relation to Control. Mean ± SEMs and mean values are shown. **d**. Progenitor cells were grouped (A-G) according to the number of progeny cells, as shown in Table 1. The cell-doubling times of each group of cells were then determined to perform Student's *t*-tests; *p<0.05, ***p<0.001 and ****p<0.0001 in relation to Control. Mean ± SEMs are shown.

Fig. 6 Analysis of reproductive ability of Control and MNNG1-exposed cells.

An *in silico* synchronized-cell lineage database was used. **a, b.** The number of progeny produced from a progenitor at 3500 mins was determined. **a.** Student's *t*-tests were performed; ns: not significant and ***$p<0.01$. Mean ± SEMs are shown. **b.** Percentages of progenitor and GD cells that produced 7–8 progeny are shown. Progenitor cells that produced 1–2, 3–4, 5–6 and 7–8 progeny were designated as Groups *A*-*D*, respectively. **c.** The number of progeny produced by GD cells in groups *A*-*D* are shown. The number of progeny produced from each group of progenitor cells are highlighted in blue. The values represent the total number of progeny produced by each group of GD cells.

Table 1. The number of progeny produced from a progenitor cell and the mean cell-doubling time

Group: No of progeny[1)]	Control		MNNG1		MNNG2		MNNG5	
	% [2)]	Doubling Time (h)[3)]	%[2)]	Doubling Time (h)[3)]	%[2)]	Doubling Time (h)[3)]	%[2)]	Doubling Time (h)[3)]
		Doubling Time (h)[4)]		Doubling Time (h)[4]		Doubling Time (h)[4]		Doubling Time (h)[4]
A: 0–2	37.50	37.1 ± 54	39.42	30.0 ± 16	80.31	nd	96.50	nd
		40.1 ± 0.9		***34.7 ± 0.5*** [****]		***35.6 ± 0.7*** [****]		***43.2 ± 2.5***
B: 3–5	17.12	34.3 ± 14	12.93	36.0 ± 16	9.55	nd	2.50	nd
		39.6 ± 0.6		***38.9 ± 0.6***		***36.9 ± 0.7*** [**]		***41.6 ± 1.9***
C: 6–8	14.35	31.7 ± 24	9.15	34.0 ± 13	3.72	NA	1.00	NA
		37.3 ± 0.4		***37.7 ± 0.5*** [*]		***36.5 ± 1.0*** [*]		***34.6 ± 1.5*** [*]
D: 9–11	11.57	34.4 ± 12	11.36	33.9 ± 9.2	3.19	NA	0	nd
		38.1 ± 0.4		***35.9 ± 0.3*** [*]		***37.5 ± 0.9***		***0***
E: 12–14	8.33	36.0 ± 14	7.89	32.6 ± 8.7	2.17	NA	0	nd
		37.3 ± 0.4		***34.4 ± 0.3*** [****]		***33.8 ± 0.7*** [****]		***0***
F: 15–17	6.48	36.0 ± 8.7	7.57	31.6 ± 5.9	0.53	NA	0	nd
		36.6 ± 0.4		***33.9 ± 0.3*** [****]		***33.4 ± 1.0*** [*]		***0***
G: ≥ 18	4.65	31.4 ± 8.6	11.68	29.6 ± 5.9	0.53	nd	0	nd
		33.0 ± 0.4		***31.2 ± 0.2*** [***]		***36.9 ± 1.2*** [***]		***0***
Total	100		100		100		100	

[1)] Progenitor cells were grouped (Group A-G) by the number of progeny produced at time 8500 min.

[2)] The % of progenitor cells that produced the number of progeny shown in the "Group: No of progeny" column is shown.

[3)] The mean cell-doubling times and standard deviations that were determined using the Gaussian distribution are shown.

[4)] The mean cell-doubling times and SEMs were calculated using the cell-doubling times of each cell.

[5)] nd: not determined.

Student's *t-tests* were performed; *$p < 0.05$, **$p < 0.01$, ***$p < 0.001$ and ****$p < 0.0001$ in relation to Control.

Supplementary Movie S1.

A time-lapse movie (time 1-850, one FOV) of HeLa cells (Control) is shown.

Supplementary Movie S2.

A time-lapse movie (time 1-850, one FOV) of HeLa cells (MNNG1) is shown.

Supplementary Movie S3.

A time-lapse movie (time 1-850, one FOV) of HeLa cells (MNNG2) is shown.

Supplementary Movie S4.

A time-lapse movie (time 1-850, one FOV) of HeLa cells (MNNG5) is shown.

Supplementary Movie S5.

A time-lapse movie (time 1-93, one FOV) of HeLa cells exposed to 40 μM of MNNG is shown.

Supplementary Fig. S1.

Cell lineage maps (Control) are shown. Light blue circle: MI, orange circle: CF, pink square: CD, blue square: incomplete cell division, black vertical line: BD and red vertical line: TD.

Supplementary Fig. S2.

Cell lineage maps (MNNG1) are shown. Light blue circle: MI, orange circle: CF, pink square: CD, blue square: incomplete cell division, black vertical line: BD and red vertical line: TD.

Supplementary Fig. S3.

Cell lineage maps (MNNG2) are shown. Light blue circle: MI, orange circle: CF, pink square: CD, blue square: incomplete cell division, black vertical line: BD and red vertical line: TD.

Supplementary Fig. S4.

Cell lineage maps (MNNG5) are shown. Light blue circle: MI, orange circle: CF, pink square: CD, blue square: incomplete cell division, black vertical line: BD and red vertical line: TD.

Fig. 1

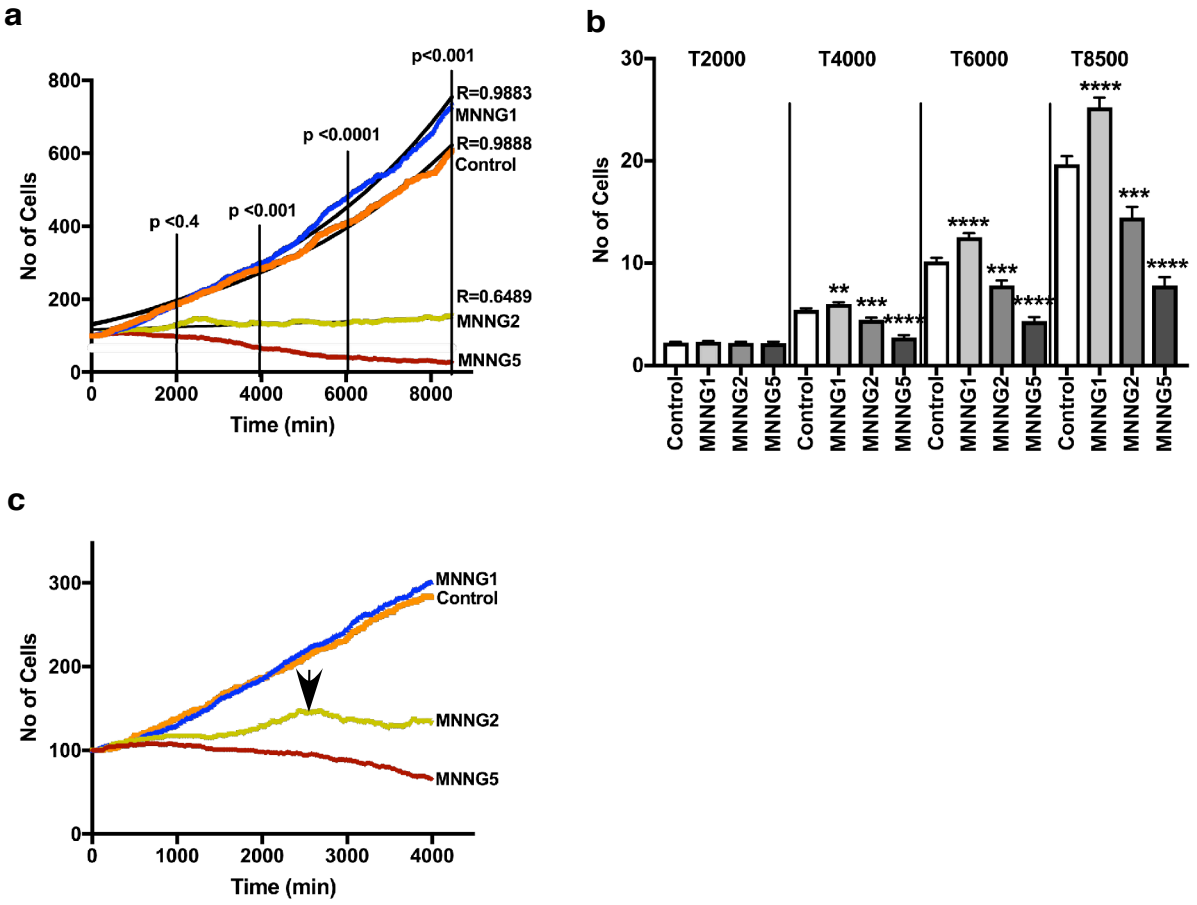

Rancourt et al.

Fig. 2

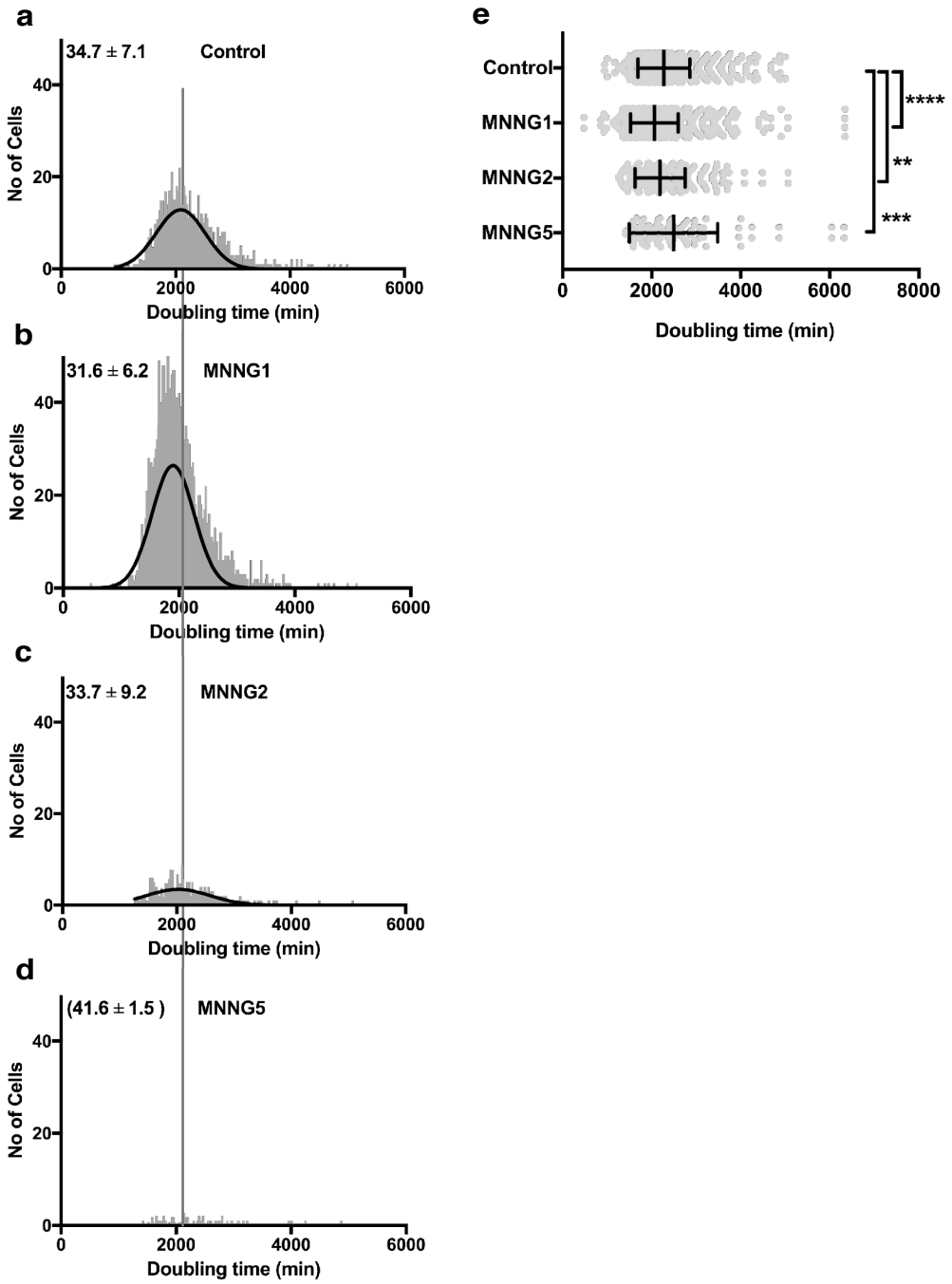

Rancourt et al.

Fig. 3

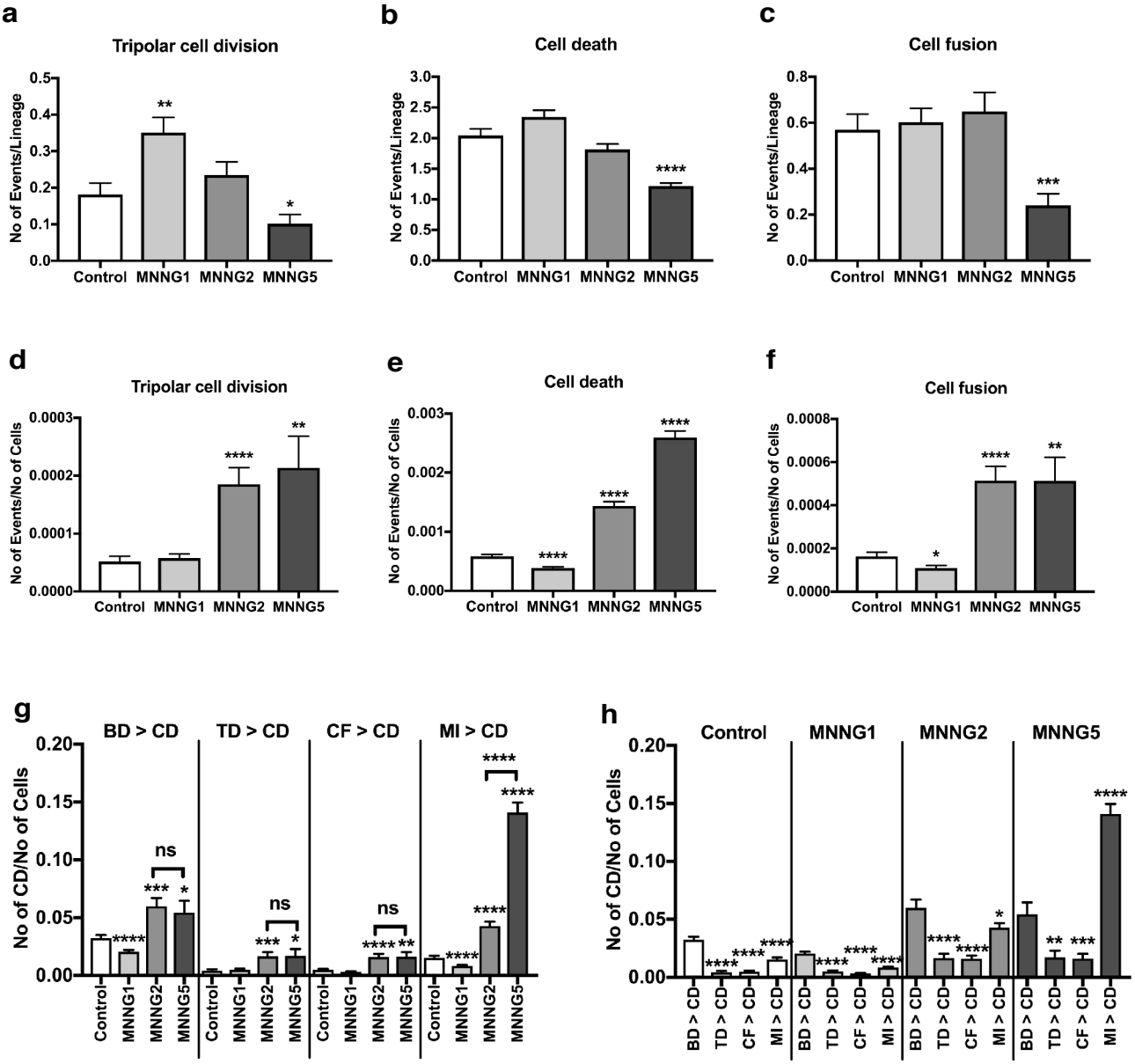

Rancourt et al.

Fig. 4

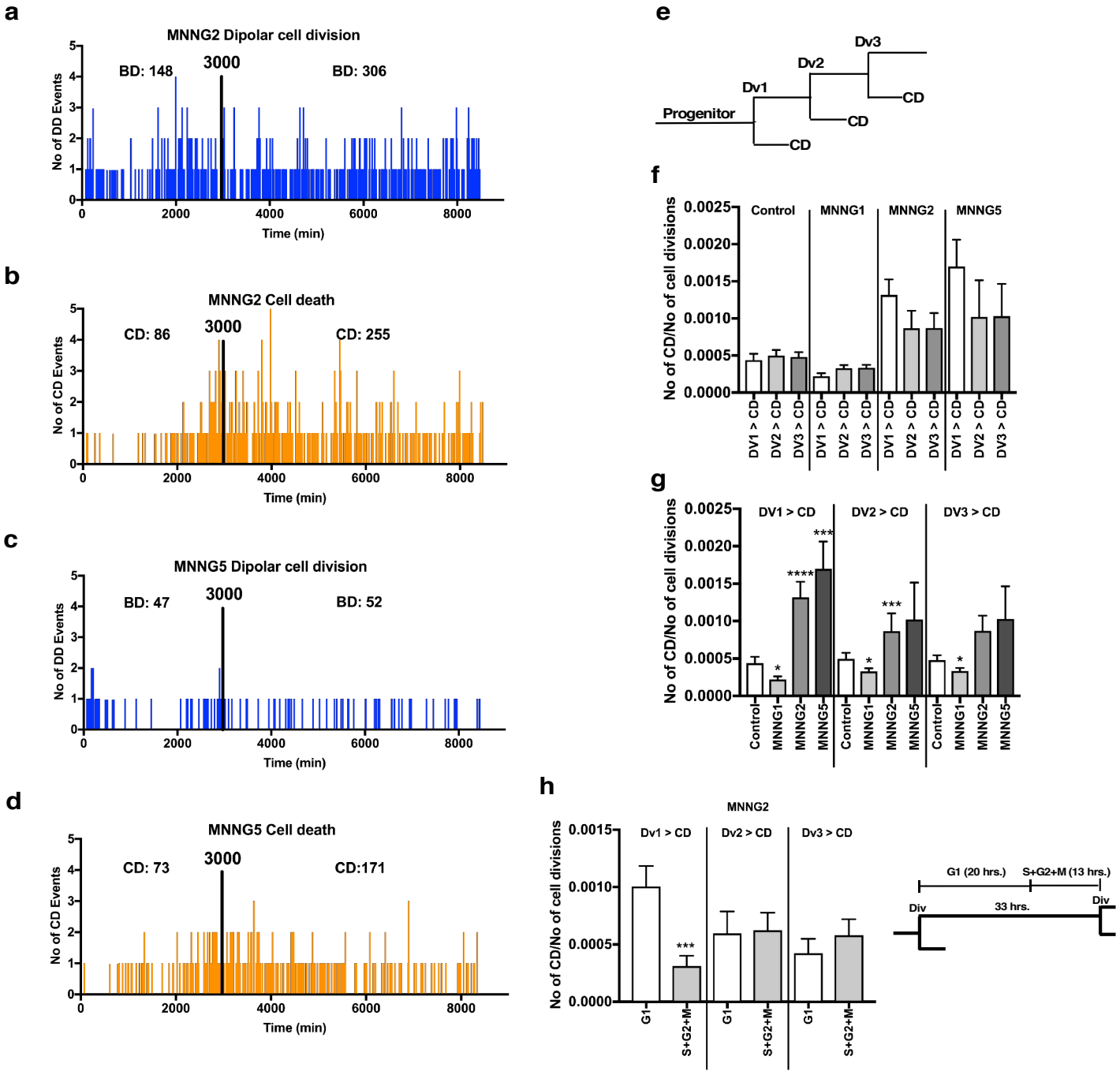

Rancourt et al.

Fig. 5

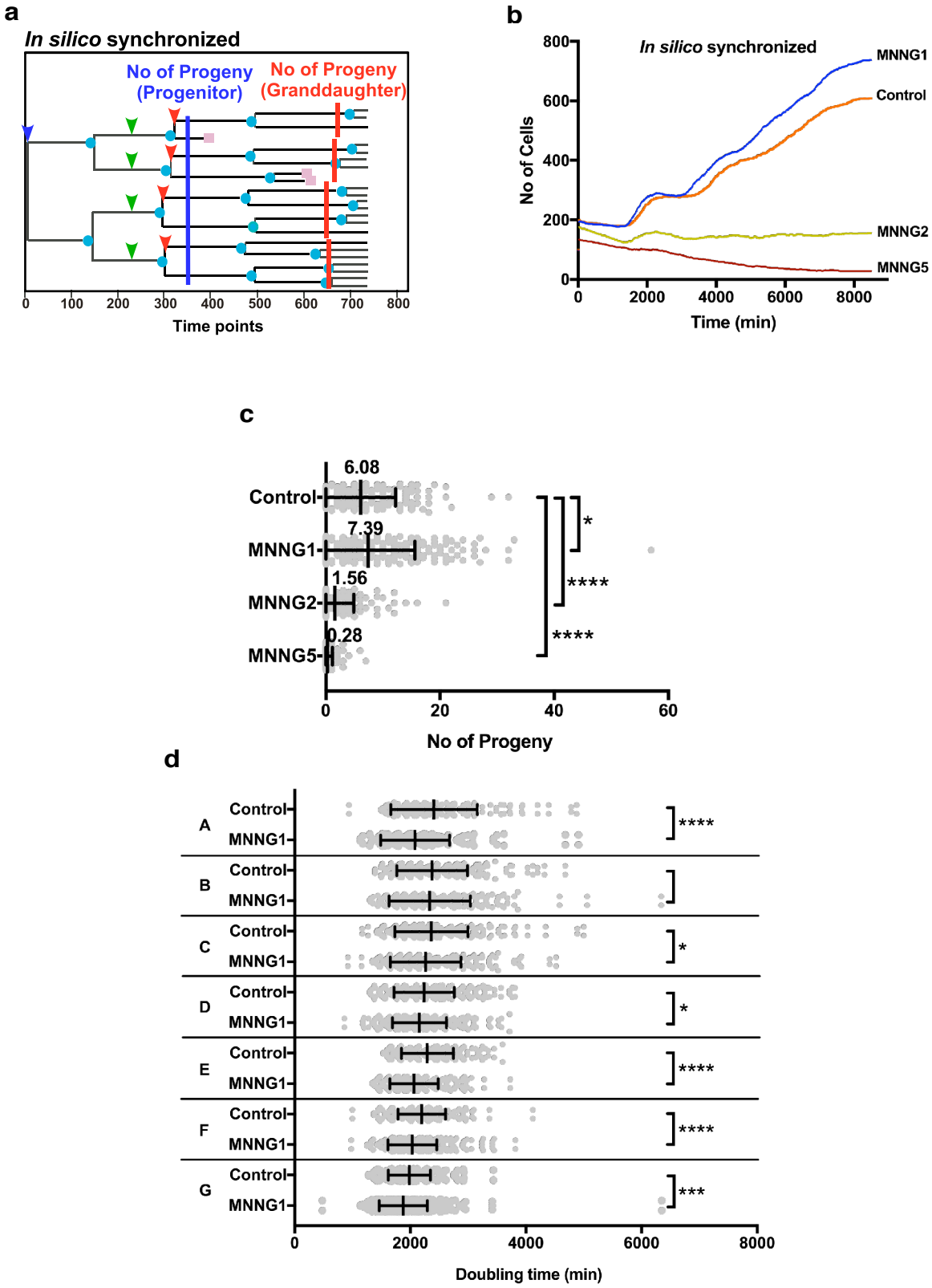

Rancourt et al.

Fig. 6

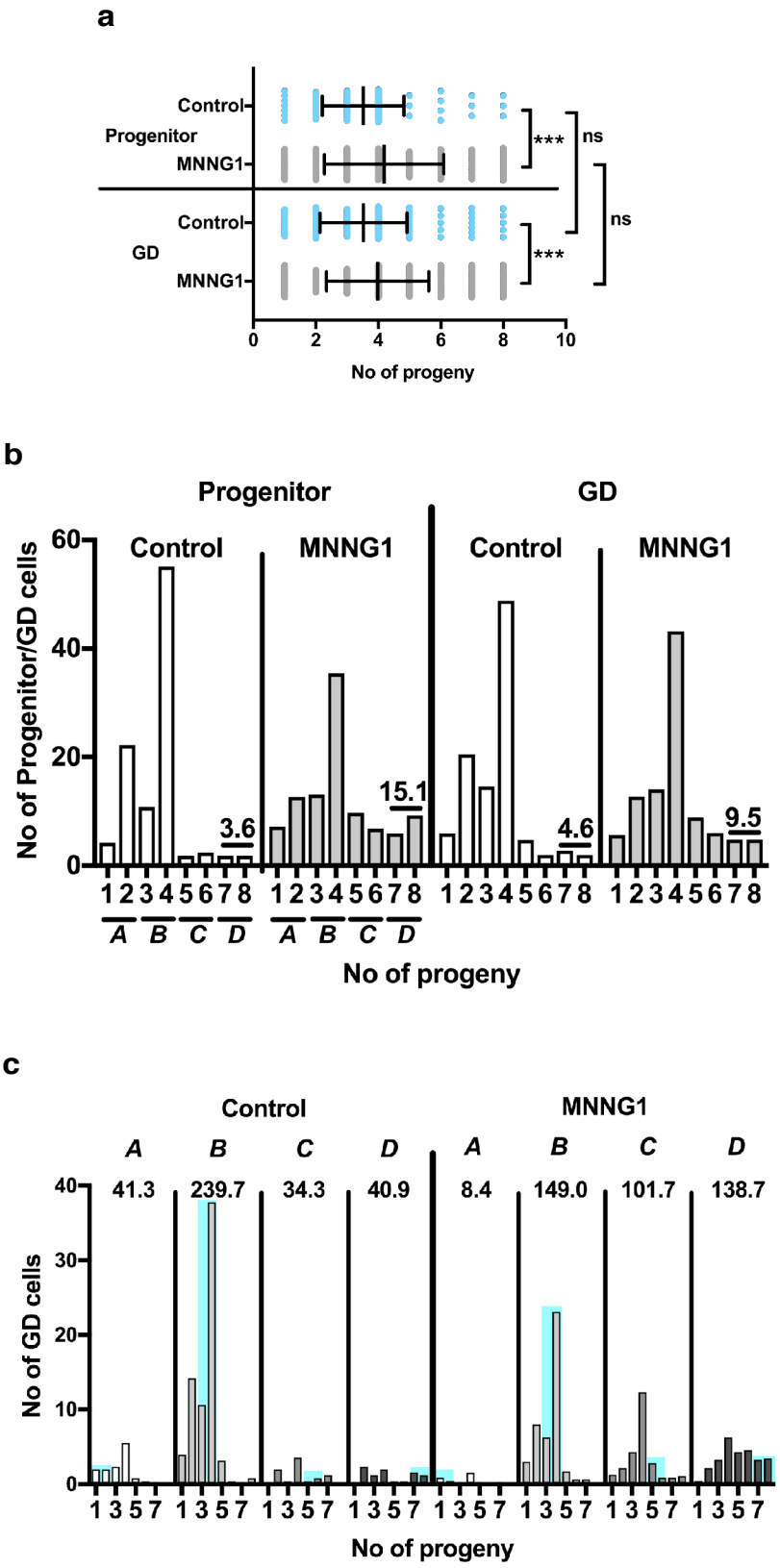

Rancourt et al.